This is an open access article published under a Creative Commons Non-Commercial No Derivative Works (CC-BY-NC-ND) Attribution License, which permits copying and redistribution of the article, and creation of adaptations, all for non-commercial purposes.

ACS AUTHORCHOICE

ACS OMEGA

http://pubs.acs.org/journal/acsodf

Article

Liquid Wicking in a Paper Strip: An Experimental and Numerical Study

Subhashis Patari and Pallab Sinha Mahapatra*

Cite This: *ACS Omega* 2020, 5, 22931−22939

Read Online

ACCESS | Metrics & More | Article Recommendations

ABSTRACT: In this decade, paper-based microfluidics has gained more interest in the research due to the vast applications in medical diagnosis, environmental monitoring, food safety analysis, etc. In this work, we presented a set of experiments to understand the physics of the capillary flow phenomenon through paper strips. Here, using the wicking phenomenon of the liquid in porous media, experimentally, we find out the capillary height of the liquid in filter paper at different time intervals. It was found that the Lucas−Washburn (L−W) model, as well as the evaporation model, fails to predict the capillary rise accurately. However, the detailed numerical solution shows a better similarity with the experimental results. We have also shown the different regimes of the wicking phenomenon using scaling analysis of the modified L−W model. The capillary rise method was applied to detect the added water content in milk. We used milk as a liquid food and found the added water content from the change in the capillary height at different concentrations of milk. Finally, results obtained from the paper-based device were verified with the commercially available lactometer data.

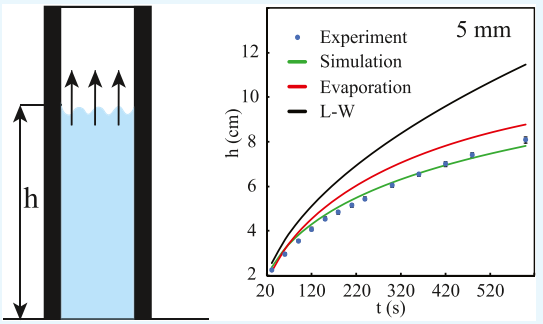

INTRODUCTION

Over the last few decades, microfluidics has been attracting increasing research interest due to the widespread applications in science and technology. Microfluidics deals with the study of fluid manipulation in microchannels. Open surface microfluidics, specifically droplet-based microfluidics, is a subgroup of classical microfluidic studies. Different types of open surfaces are used in microfluidic applications such as metal,[1] plastic,[2,3] paper,[4] fabric,[5] etc. Paper-based devices have various applications in the field of healthcare diagnosis, environmental monitoring, food quality control, biomedical applications,[6−10] etc. Whatman filter paper is used in most of the research studies because it is easily available, cheap, thin, lightweight, disposable, biodegradable, and easy to store and transport.[11] In 2007, Whitesides and his group[4] first used paper as a microfluidic device. They also came up with new fabrication processes and different bioassay identification techniques using a paper microfluidic device.[12−15] Liquid manipulation is important for making a paper-based device, and it can be easily controlled in a porous substrate by making patterned (hydrophilic−hydrophobic) surfaces.[16] Chatterjee et al.[17] showed the lateral and transverse transport of liquid experimentally on a paper-based substrate using wettability patterning. Using the concept of liquid manipulation by making patterned surfaces and colorimetric reactions, paper-based microfluidic devices were used to detect contamination in liquid foods such as lime juice, orange juice, tea, drinking water, whiskey, wines, etc.[18−20]

A liquid can easily flow through the gaps in porous media without using any extra energy due to the inherent capillary action. Darcy[21] first investigated the flow of liquid in porous media experimentally. In 1921, two researchers established a relationship between the capillary height and rising time of a liquid in porous media popularly known as the Lucas−Washburn (L−W) equation.[22] Using the concept of the L−W model, various studies had been done to understand the physics of liquid wicking in porous media. The L−W model scales the liquid wicking distance (x) with time (t) as $x \sim t^{1/2}$. However, this model failed to predict the experimental results of the liquid wicking phenomenon in porous media for a long time interval. Schoelkopf et al.[23] observed the deviation of the L−W model in the case of liquid imbibition through porous media. They also concluded that in a very short time interval, the inertial effect dominated the capillary flow considering no change in the surface properties and geometry. Fries et al.[24] modified the L−W model for wicking of highly volatile liquids in porous media, including the evaporation effect. They found a good agreement between the experimental and analytical

Received: May 22, 2020
Accepted: August 17, 2020
Published: September 1, 2020

Downloaded via 136.226.50.81 on December 19, 2024 at 04:33:50 (UTC).
See https://pubs.acs.org/sharingguidelines for options on how to legitimately share published articles.

© 2020 American Chemical Society

https://dx.doi.org/10.1021/acsomega.0c02407
ACS Omega 2020, 5, 22931−22939

RAI Exhibit 2010
Shenzhen Kangvape v. RAI
IPR2024-01406

results. They showed that the capillary rise is inversely proportional to the evaporation rate. Hamdaoui[25,26] also developed an analytical model considering the gravity effect on the wicking phenomenon. They showed that the generalized L−W model could be used in the case of short and long time experiments. Li et al.[27] proposed the criteria of using the L−W model in the case of spontaneous imbibition of a liquid in porous media. They also described the criteria of including the effect of gravity on wicking using the CGR number (capillary pressure-to-gravity force ratio). Chang[28] discussed an experimental and theoretical study on the dynamics of water flow through a paper with swelling. They considered the expansion of intrafiber pores as well as interfiber pores, which leads to paper swelling at the time of water imbibition. Flow through porous media is dependent on the properties of the media such as porosity, permeability, etc. One of the important approaches was combining the properties of porous media with the L−W model considering Darcy's law.[29] Despite these various approaches, there are still difficulties in understanding the dynamics of liquid imbibition through porous media because of the three-phase complex formation of solid−liquid and −gas interfaces. As a result of this complex geometry, the deviation of the theoretical and experimental data is expected. Numerical simulation can be an option to overcome the drawbacks of analytical studies. Rath et al.[30] developed a relation among the capillary pressure, permeability, and saturation in the case of liquid imbibition through porous media. They also demonstrated numerical simulation using Richard's equation to model the imbibition process. Using the capillary-driven flow concept, Rayaprolu et al.[31] developed a paper-based device to measure the viscosity of Newtonian and a few non-Newtonian fluids. Recently, Kar et al.[32] reviewed a few applications of paper-based microfluidic devices, including blood plasma separation, green energy harvesting, etc. They described the fundamental of capillary-driven transport of a liquid in the paper substrate considering the single capillary tube theory (with or without gravity), Darcy's law-based model, and Richard's law-based model.

In this work, we performed experimental and numerical studies on liquid wicking in a paper strip. This study included the experimental findings of porosity, permeability, capillary rise, and capillary radius of Whatman filter paper (grade 4). We presented a general hydrodynamic framework for liquid imbibition into the porous matrix. To explain the physics of the capillary rise phenomenon, we analyzed the experimental and numerical data with the L−W model and the evaporation model. The relation between the capillary rise of different liquids in paper strips with wicking time using the Lucas−Washburn (L−W) model, evaporation model, and numerical simulation was shown. The COMSOL multiphysics environment was used to perform the numerical analysis using Darcy's law with gravity. We also showed a scaling analysis of liquid wicking in a paper strip using a modified L−W model. The wicking phenomenon was divided into three different regimes, considering the inertial effect (Regime I), viscous effect (Regime II), and gravitational effect (Regime III), and compared with the experimental results. From the simulations and the analytical methods, it was seen that gravity plays a role particularly at the later stage of the imbibition. The simple method presented in this paper can be used to develop a paper-based microfluidic device to detect liquid food adulteration. We also used this method to find out the added water content in milk. Finally, the predicted data from the experiments were compared with those from the commercially available lactometer to measure its accuracy. To the best of our knowledge, we have shown for the first time the detailed numerical solutions for the capillary rise of liquid in a paper-based substrate and compared with the experiments and analytical methods for milk. This method can be used efficiently for other liquid foods or even chemicals to identify the amount of water.

■ RESULTS AND DISCUSSION

In this study, we observed the capillary flow of water and milk in a paper strip. Two properties that lead to liquid flow in porous media are wettability and wicking. Due to wettability, first the porous surface wets and helps the liquid to wick through the porous media. Due to the effect of negative capillary pressure, the wicking of liquid occurs in porous media spontaneously. Although paper consists of randomly oriented fibers, Lucas−Washburn[22] first model the wicking phenomena by considering paper as bundles of capillary tubes. Darcy[21] explained the wicking phenomena in porous media by considering a single-phase and a two-phase flow. These mathematical models were developed by solving the conservative equations considering the effect of different forces such as pressure, inertia, viscosity, and gravity. The details of the capillary flow models are described in the Experimental and Numerical Procedures section. The results of capillary rise from the experimental study, numerical modeling, and analytical models were compared in water and milk. The effect of different concentrations of milk on the capillary rise was analyzed to identify the added water content in the milk sample. Last, we observed the paper strip prediction and that of the lactometer for finding the amount of dilution in milk.

Capillary Rise of Water in a Paper Strip. In Figure 1a, we show the capillary rise of water in a 20 mm width filter paper using the L−W model, evaporation model, numerical simulation, and experiments. Here, we used capillary radius (R_c) as half of the pore diameter (25 μm) that is given by the manufacturer. However, the experimental results do not match with the numerical results. Ravi et al.[33] described a method to find out the capillary radius using the capillary pressure generated by reference liquids and a test liquid as *n*-hexane and water, respectively. Masoodi et al.[34] described another method of finding the capillary radius of porous media, which we used and modified the capillary radius. They used different polymer wicks and different liquids to perform wicking experiments. By balancing the upward suction force and downward gravitational force, the capillary radius can be expressed as

$$R_c = \frac{2\gamma \cos(\theta)}{\rho g L_{ss}} \tag{1}$$

where R_c is the capillary radius, γ is the surface tension of the liquid, θ is the static contact angle, ρ is the density of the liquid, g is the gravitational acceleration, and L_{ss} is the saturated capillary rise height. Using these values of R_c from eq 1, we modified the numerical results. The modified results of liquid wicking for a 20 mm width paper strip are shown in Figure 1b. It can be seen that after modifying the capillary radius, the prediction of the simulation matches very well with the experimental findings.

The average capillary rise at each time interval for different width paper strips was found by performing multiple experiments. Experimental results of the capillary rise were

https://dx.doi.org/10.1021/acsomega.0c02407
ACS Omega 2020, 5, 22931−22939

RAI Exhibit 2010
Shenzhen Kangvape v. RAI
IPR2024-01406

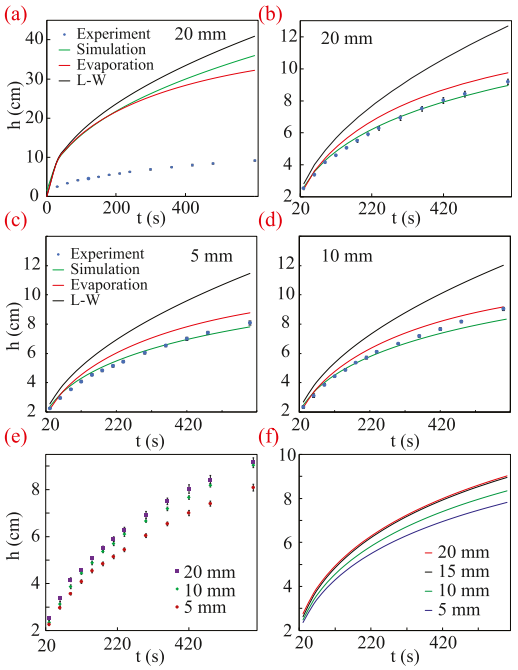

Figure 1. Comparison of the experimental, numerical, and analytical data is shown for capillary rise of water in paper strips. (a) In a 20 mm paper strip comparing all of the results by taking capillary radius as half of the pore diameter. Taking the modified capillary radius from eq 1, the comparison is done for paper strip widths of (b) 20 mm, (c) 5 mm, and (d) 10 mm. (e) Repeatability of the capillary rise experiments for three different paper strip widths. (f) Simulated results of capillary rise for different width paper strips are shown to find out the effect of width size. In the case of 20 mm width, the rise is maximum, and in case of 5 mm, the rise is minimum.

compared with the simulated data, L−W model, and evaporation models. In Figure 1c,d, the capillary rise of water in paper strips with respect to time is shown for different widths. The experimental and the simulated data show almost similar results, whereas the data from the L−W model and evaporation model deviate from the experimental results. The reason behind this is that in the case of the L−W model, the capillary height (h) is varying with time (t) as $h \propto t^{0.5}$, which is not valid for a more extended time because of the retardation in liquid flow velocity due to viscous resistance. In the case of the evaporation model, the deviation is less because we considered the loss due to evaporation. The capillary tube theory is also considered in the evaporation model. However, there is a deviation with the experimental results because the paper strip is not consisting of bundles of capillary tubes. In capillary tube theory, a porous medium is described as a bundle of similar capillary tubes.[35] Although there is a quantitative deviation in results, the trend of the graph is same. The simulated data are closely following the experimental results. In the numerical simulation, we considered the porous medium subsurface flow module without considering the capillary tube theory. For liquid velocity, we used Darcy's law, and for capillary pressure, we used the Brooks and Corey model, which are based on the flow of porous media. The simulation environment is almost the same as the working conditions. Therefore, the predicted data from the simulation show similar results to the experimental data.

In Figure 1e, we compared the capillary rise height of pure water using different strip widths at a different time interval. Zhong et al.[36] and Jafry et al.[37] showed that there is no effect of paper strip width on liquid wicking if the strip width is minimal. They found that in the range of 1.2−2 mm width of the paper strip, the variation of liquid velocity is minimal. In eq 13 also, there is no effect of strip width because of considering an infinite width strip. However, it is clear from Figure 1e that the capillary rise is increasing with an increase in the width size. Due to the wider strip, the boundary effect is less than that in the thinner strip. In the side boundaries, the presence of the solid−air interface causes stronger viscous resistance due to the downward surface tension force. Therefore, if the strip is wider, the resultant surface tension force is lower compared to that in a thinner strip. Also, in the case of a wider strip, more amount of liquid is sucked into the strip. Due to more volume, the liquid spreads more, and the height is increased.[38] In Figure 1f, we show the effect of width size on capillary rise using numerical simulation. It is clear from the figure that on increasing the width size, the height is increasing because of less boundary effect. In Figure 1f, we can see that there is almost negligible change in the height in the case of 15 and 20 mm width paper strips. Therefore, from this, we can conclude that if the strip width is more than 20 mm, the boundary effect is negligible. In Figure 2a, it can be seen that for the first few

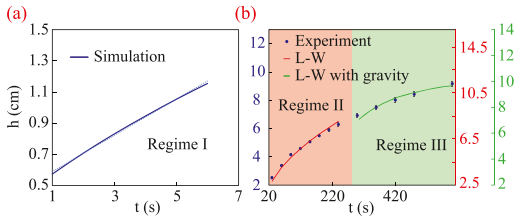

Figure 2. (a) Comparison of numerical simulation and analytical data of water wicking in a paper strip. Regime I of the wicking process is shown. (b) Comparison of experimental and analytical data of water wicking in a paper strip. Two regimes (Regime II and Regime III) of the wicking process are shown here. It has been shown in Figure 1 that the experimental values and the L−W predictions do not match. Here, the scaling of the L−W model considering only the viscous term in Regime II and the scaling of L−W model including the gravity term in Regime III match well with the trend of the experimental data.

seconds, $h \sim t$. In the initial phase of imbibition, the inertial force balances the capillary force, and an inertial regime (Regime I) of flow is observed. From the scaling of inertial and capillary forces, it can be shown that

$$h \sim \left(\frac{2\gamma}{\rho R_c}\right)^{1/2} t \tag{2}$$

The other two regimes of liquid imbibition are shown in Figure 2b. Regime II is the Lucas−Washburn (L−W) regime, and the scaling of viscous and capillary forces gives $h \sim t^{1/2}$. It can be seen from Figure 2b that the trend of Regime II matches very well with the L−W prediction. In the last part of the imbibition process, gravity dominates the spontaneous spreading of liquid on the paper strip. In Regime III, the capillary height can be calculated using eq 20, which is discussed later. It can be seen from Figure 2b that the trend of Regime III matches very well with the L−W prediction, including the gravity term. The objective of showing the analytical results for the viscous and capillary effect (in Regime II) and gravity effect with the L−W

https://dx.doi.org/10.1021/acsomega.0c02407
ACS Omega 2020, 5, 22931−22939
RAI Exhibit 2010
Shenzhen Kangvape v. RAI
IPR2024-01406

model (in Regime III) in the secondary axis is to show the trends of the regimes. The figure clearly shows the trend of the experimental values, and the analytical results match well, although from Figure 1, it is clear that the experimental values and the L−W predictions do not match.

Capillary Rise of Milk in a Paper Strip. Milk contains more than 80% of water. Therefore, milk can also smoothly flows through porous media. We performed a similar experimental, analytical, and numerical study of milk wicking in a paper strip. The comparison of these studies was made for a commercial milk (Amul milk) considering a 20 mm paper strip. In Figure 3a, we can see that the L−W model data and

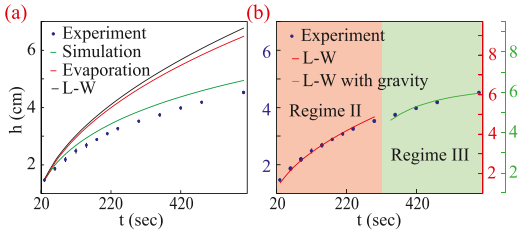

Figure 3. (a) Comparison of capillary rise of Amul milk with a 20 mm width paper strip, showing the different results from the L−W model, evaporation model, and COMSOL simulation and comparison with experimental data. (b) Comparison of the experimental and analytical data using the scaling of the L−W model considering only the viscosity effect in Regime II and gravity effect in Regime III. The predicted values of the L−W model and L−W with gravity are shown in the secondary axis to confirm the data trend. It can be seen from (a) that the analytical data fails to predict the experimental results.

evaporation model data deviate more from the experimental results. The reason is the same as explained earlier. The evaporation model data is more close to L−W model data because the evaporation rate is less in the case of milk. The different values of the parameters that are used in the case of milk are listed in Table 1.

Table 1. Parameters Used for Milk Testing

name	value
surface tension	0.049 N/m
capillary radius	0.160 mm
density of milk	1030 kg/m^3
viscosity of milk	17.9 × 10^{-4} Pa·s
milk saturated pressure	4242.85 Pa
latent heat of vaporization	16 173.25 kJ/kg

The simulated data for the capillary rise of milk also does not exactly match the experimental results. All of the properties of the milk are considered as fixed. However, milk is an emulsion and colloidal properties are required to model for better prediction of the behavior of milk. The microscopic behavior of the milk wicking phenomenon is difficult to predict by numerical simulations. There is a possibility of blocking of the pores of the paper strip due to the solid content (10−15%) of the milk. Even the multiphase simulation approach may be required, which is the future scope of the current work. Therefore, the deviation of the experimental and simulation data is expected. However, the trend is almost similar to that of the experiments. In Figure 3b, different regimes of imbibition are shown. The inertia-dominated Regime I is not shown here. As explained earlier, Regime II is the viscous-force-dominated regime and follows the trend of L−W law where $h \sim t^{1/2}$. Regime III is the slow gravity-dominated regime. It can be seen from Figure 3b that the scales for both the regimes match very well with the experimental data. A detailed description of the experimental processes for identification of the water content in milk is discussed in the next section.

Water Content in Milk. For finding the added water content in the milk, we used a paper strip whose schematic is shown in Figure 4a. We used hydrophobic ink to make barriers

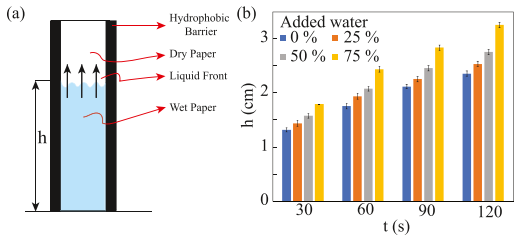

Figure 4. (a) Schematic of the paper strip for measuring the capillary height. (b) Change in the capillary height due to change in the water concentration at four different time intervals. Four different colors are showing the different concentrations of added water at a particular time. With the increase of the water concentration, the capillary height is also increased.

in the side boundaries for making the flow more controlled, and we put the scale bar on the hydrophobic barriers (flow width is 10 mm). There is an effect of hydrophobic barriers on the rising height because of an increase in viscous resistance. Hong et al.[39] described a detailed study on the effect of the wax barrier in the case of wicking height. Jafry et al.[37] discussed a comparative study of the barrier effect. They used Whatman filter paper grade 1 and made a hydrophobic barrier using wax and SU-8. We used a commercially available Amul milk as a sample and measured the capillary height with respect to time. Then, we added different volumes of water in the pure milk and found the changes in capillary heights. Due to the increased amount of water, the capillary height is also increased. After multiple experiments, we took the average values of heights at different time intervals and mark them for detection of 25, 50, and 75% added water. In Figure 4b, we can see the changes in the capillary rise at different milk concentrations.

We used a commercially available lactometer to compare our results for checking the accuracy of the paper-based detection technique. We calibrated the lactometer using samples of varying concentrations of Amul milk using 0, 25, 50, and 75% added water. We noted down the change of height in the paper strip and lactometer for different concentrations of milk. Paper strip data are taken at a fixed time interval for all of the four different concentrated milk samples. From these successive experimental results, we plotted a graph between the height and % of water content for the lactometer and paper strip. We used those data as a reference and fitted a second-order polynomial curve to the reference values with a regression of 0.9937 for paper and 0.9975 for the lactometer. The equations of the calibration curves are $y = 1.28x^2 + 0.208x + 2.372$ and $y = 1.1429x^2 + 28.857x + 0.1429$ for the paper strip and lactometer, respectively, where y represents the capillary height and x represents the % of added water content in the milk sample. Further, we used these equations of the fitting curves to find out the added water content in milk. We measured the readings from the paper strip as well as from the lactometer for

https://dx.doi.org/10.1021/acsomega.0c02407
ACS Omega 2020, 5, 22931−22939
RAI Exhibit 2010
Shenzhen Kangvape v. RAI
IPR2024-01406

samples with random volumes of water and put these in the fitting curve equations. The comparison of both the readings is shown in Figure 5. From the figure, it is clear that the

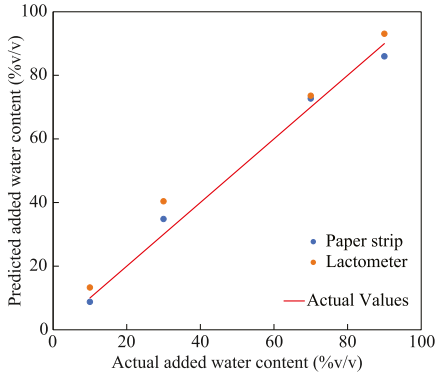

Figure 5. Comparison between the lactometer readings and paper strip readings (after 2 min). The actual values of the water content are shown by the red line.

predictions of the paper strip and the lactometer are close to the original added water content. The maximum deviations of the predicted readings from the actual readings in the case of lactometer and paper strip are 34.7 and 16.2%, respectively.

■ CONCLUSIONS

Despite the considerable amount of literature on the capillary rise of liquid on a porous substrate, the analytical models are not able to predict the capillary rise on the paper-based substrate accurately. In this work, we discussed the wicking phenomenon of liquid in Whatman grade 4 filter paper. We explained the physics of the well-known capillary rise of water on the paper-based substrate through experimental results, simulations, the L−W model, and the evaporation model. Apart from the fundamental understanding of the capillary rise of liquid on a porous substrate, this work demonstrates a method for practical applications. The present hydrodynamic model can be modified to study more complex phenomena. Some examples are the evaporation effect during the spreading of a volatile liquid, liquid imbibition in soil, thermal characteristics during the spread of liquid, etc.

Along with the fundamental understanding, the concept of capillary rise in porous media is used to detect contamination in liquid foods such as milk with water. We measured the changes in capillary heights due to the different concentrations of milk. The technique mentioned above of detecting water content using the paper-based substrate can pave the way for identifying adulterants in any liquid food sample like oil, liquor, juice, etc. A similar process can be used for determining the liquid components in chemical mixtures.

■ EXPERIMENTAL AND NUMERICAL PROCEDURES

Materials. Whatman filter paper (grade 4) is used in this study. We cut it into different rectangular shapes. We have used a screw gauge to measure the thickness of the paper. As liquid samples, we have used deionized water and commercially available Amul milk (3.1% fat content). Experiments were performed in a controlled environment of known temperature (26 ± 1 °C) and relative humidity (70%). The properties of the materials such as density and pore size were taken from the standard chart. Few other properties such as porosity, permeability, capillary radius, thickness of paper, viscosity, and surface tension of the sample, etc. were measured by performing experiments, which are discussed later. The different values of all of these properties are mentioned in different tables in this paper.

Experimental Study. For performing the control experiments, the paper strip must be held in a vertically upward direction. To hold the paper, we made a setup as shown in Figure 6a. The holding setup is made of aluminum. It has a

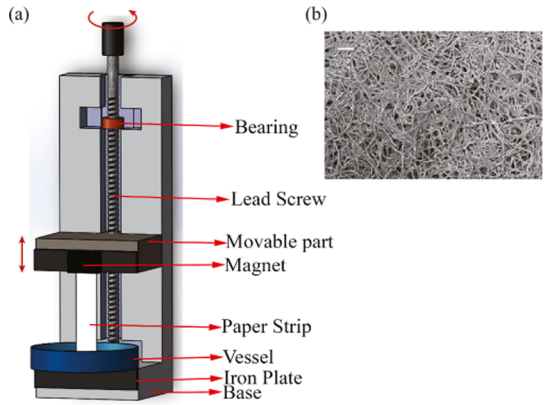

Figure 6. (a) Schematic of the experimental setup, which includes different parts such as bearing, lead screw, iron plate, magnets, etc. (b) SEM image of Whatman filter paper grade 4. Reprinted (adapted) with permission from ref 32. Copyright (2020) American Chemical Society.

rectangular base and two rectangular blocks, which are connected perpendicularly to the base. Of these two blocks, one is fixed to the base and one is connected to a lead screw. With the help of the lead screw, one block can move up and down for the purpose of adjustment of the paper strips. We attached small rectangular iron plates on the aluminum block using screws. Small magnets are used to hold the paper strips on the iron plates. We attached a scale bar with the paper strips to measure the capillary height. The samples are taken in a measuring jar and put at the bottom of the paper strip. The scanning electron microscopy (SEM) image of Whatman filter paper grade 4 is shown in Figure 6b. For taking videos and photos, we used a DSLR camera (Nikon D750), which is held in front of the setup. A level is marked in the paper strip indicating the level of dipping of the paper strip in the sample. We moved the lead screw slowly downward and stopped when the paper strip mark touched the sample surface. Then, we started the timer and took reading at different intervals of time. The maximum error in taking the readings was ±1 mm. The uncertainties of the measured values are listed in the Table 2. We have considered 99% confidence level to determine the

Table 2. Uncertainty of the Measured Values

name	margin of error
capillary height	1 mm
paper strip width	±3.64%
paper strip thickness	±0.23%
wicking liquid mass	0.001 g
porosity	±5.98%
permeability	±12.2%
viscosity of liquid	1%

https://dx.doi.org/10.1021/acsomega.0c02407
ACS Omega 2020, 5, 22931−22939

RAI Exhibit 2010
Shenzhen Kangvape v. RAI
IPR2024-01406

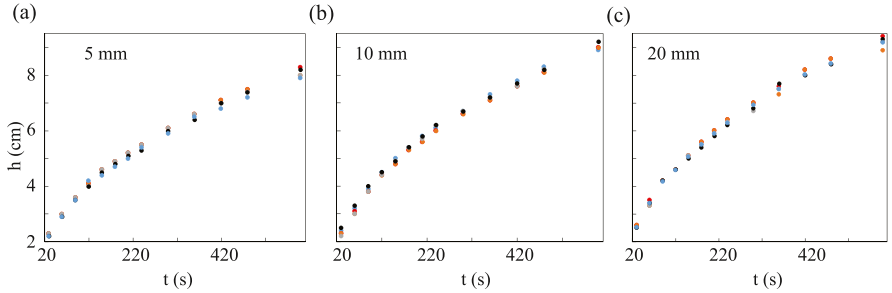

Figure 7. Graphical representation of capillary rise height and time for five repeated experiments in the case of (a) 5 mm, (b) 10 mm, and (c) 20 mm width paper strips.

errors in the measured values. The viscosity of the liquid samples is measured using a viscometer (DV-II, Brookfield), and the surface tension is measured using a goniometer (Attension Theta, Biolin Scientific). Brookfield viscometers work on the rotational viscometry principle. By measuring the torque required to rotate a spindle at a constant speed in a fluid sample, the viscosity can be measured because the torque is proportional to the viscous drag. To measure the surface tension, we used the pendant drop method. Using a needle, we make a pendant drop in front of the light source in the goniometer setup. The shape of the drop depends on the surface tension force and gravitational force. We have performed multiple experiments of capillary rise of liquid with different width size (5, 10, and 20 mm) paper strips. The repeatability of the experimental data of all of the three different width paper strips is shown in Figure 7. The different time intervals are shown on the *X*-axis, and the capillary rise is shown on the *Y*-axis. With time, the capillary height also increases. We took reading up to 10 min and move the lead screw upward until the paper strip separated from the sample. We took five repeated data of capillary rise for each paper strip under the same operating conditions. The maximum deviation ($\Delta = ((\max - \min)/\max) \times 100\%$) between the highest and the lowest value of height is found to be less than 10% in each case of the paper strip. We measured the capillary height using a standard scale attached to the paper strips. We have followed the process to make our measurements comparable with the lactometer reading (mentioned earlier). To test the accuracy of the method, we have also employed an image processing technique to measure the capillary length. For image processing, we converted the recorded video into images. The image was then converted from RGB to a grayscale image, and then it was further processed to remove any additional noise from it. The filtered grayscale image was later converted into its complementary form to make it easy to distinguish the milk rise from paper. Finally, the edges were detected from the cleaned complementary image using the Canny edge detection method, and the height was measured with the help of a reference scale. For example, the height measured using the image processing technique was 1.38 cm, whereas the scale height was 1.4 cm. Thus, the overall error estimated after multiple experiments and comparing it with the corresponding image processing results was around 1.5%. From these sets of experiments, we can conclude the excellent reliability of the experimental system and proceed with further investigations.

We also performed two different experiments to find out the porosity and permeability of the filter paper. Porosity is the ratio of the empty space volume inside the porous media and the total volume of the porous media. It can vary between 0 and 1. Experimentally, we measured the porosity of Whatman filter paper grade 4. Here, we used the gravimetric test method to find the mean porosity of the filter paper applying eq 3 as described in the literature.[29,38]

$$\epsilon = \frac{m_{sat}}{\rho A_{cs} L_{ss}} \tag{3}$$

where ϵ is the porosity of filter paper, m_{sat} is the mass of the water soaked by filter paper in a saturated condition, which was determined using a weighing balance (Pioneer, Ohaus), and A_{cs} is the cross-sectional area of the filter paper. For measuring the porosity, we cut the filter paper in a rectangular shape with different widths as 5, 10, and 20 mm. We have carried out five experiments for each of the paper strips. For finding m_{sat}, we measures the weight of the filter paper before and after the experiment and took the difference between the two readings. After performing multiple experiments, we got an average porosity value as 0.776, which is comparable with the earlier measurements of porosity for Whatman grade 4 filter paper.[40−42]

In porous media, the liquid flow is dependent on its permeability value. Permeability is the measurement of the ability of liquid flow through porous media. We used eq 4 to find out the permeability of Whatman filter paper grade 4. Experimentally, we obtained the unknown values of eq 4

$$\ln\left(\frac{x_o}{x}\right) = \frac{K\rho g R_w^2}{\mu L_w R_{sr}^2} t \tag{4}$$

where x_o is the initial height of the water head in the syringe, x is the final height of the water head, K is the permeability of the paper, μ is the dynamic viscosity of the liquid sample, R_w is the radius of the cylindrical filter paper, L_w is the height of the cylindrical paper, and R_{sr} is the radius of the syringe. Equation 4 is based on the falling head method used by Masoodi et al.[29] In the falling head method, permeability can be measured from the change in water head with respect to time. In this test, liquid flows through a porous medium from a source that provides the water head. With time, the water head of the source is decreased. Here, we used a syringe as a source and a filter paper (Whatman grade 4) as a porous medium. At the tip of the syringe, the paper is connected, through which the liquid can flow. We filled the syringe with water and marked a level to start. The time taken for the water head to fall by 5 mm is noted. The similar way multiple readings are taken by changing the length of the filter paper. Scale and screw gauges were used to measure all of the lengths and the diameters. From our experiments, we obtained an average permeability value of 8.67 $\times 10^{-12}$ m^2, which is comparable with the earlier results of permeability for Whatman grade 4 filter paper.[40,41] Further, we

https://dx.doi.org/10.1021/acsomega.0c02407
ACS Omega 2020, 5, 22931−22939

RAI Exhibit 2010
Shenzhen Kangvape v. RAI
IPR2024-01406

have used the same values of porosity and permeability in the numerical modeling.

Numerical Modeling. A finite element method (FEM) is used to solve the numerical problem using a COMSOL multiphysics environment. Three different physics interfaces from the porous media and the subsurface flow module are used to solve the problem. To describe the fluid movement through the porous medium, we added Darcy's law interface.[43] This physics interface can be used for the flows with low velocity, where the pressure gradient is the primary driving force. The viscous resistance force in pores is the primary counterforce in this physics. The shear stress in the side boundaries is negligible because there are no hydrophobic boundaries in the paper strip. No flow condition is applied across the vertical boundaries. A reference pressure level p_{ref} is set as 1 atm, and the initial value of the dependent variable, such as pressure p, is set to be 0 Pa. The equations used for the continuity and momentum balance (Darcy's law model) are

$$\frac{\partial(\epsilon\rho)}{\partial t} + \nabla\cdot(\rho u) = -\dot{Q}_m \tag{5}$$

$$u = -\frac{K}{\mu}(\nabla p + \rho g) \tag{6}$$

where $\dot{Q}_m$ is the mass source (rate of evaporated mass from the porous media), u is the volume-averaged Darcy velocity, and ∇p is the total pressure drop. The nonzero volumetric evaporation rate term ($\dot{Q}_m$) in the conservation equations[44,45] is considered when a large temperature difference between the atmosphere and the porous media or external airflow is present in the wicking process. The evaporated mass term is expressed as[45]

$$\dot{Q}_m = C(\rho_{v,eq} - \rho_v)s_g\epsilon \tag{7}$$

where C is the evaporation rate constant and $\rho_v = \rho_g w_v$. Here, ρ_g and ρ_v are air and vapor density, respectively, w_v is the mass fraction of vapor, and s_g is the volume fraction of air. Here, we only consider the conservation equation of water inside porous media because of the reduction in mass due to evaporation. The interface temperature can be found using the energy balance equation. In the present work, we performed the experiments under an almost constant environment without any effect of external sources. Therefore, in the current work, we have not considered the effect of evaporation; thus, $\dot{Q}_m = 0$ is assumed.

For defining the phase material and the flow transport properties, we used the phase transport at the porous medium interface.[46] Relative permeabilities and capillary pressures are taken into account to model the transport of multiple immiscible phases in a porous medium while using this physics interface. For modeling the capillary pressure in the case of two-phase flow, we chose the Brooks and Corey model[47] and denote the entry capillary pressure as p_{ec} and pore size distribution index as λ_p. For two-phase flow, Darcy's law without any mass source is defined as

$$\frac{\partial(\epsilon\rho_{s_i}s_i)}{\partial t} + \nabla\cdot(\rho_{s_i}u_i) = 0 \tag{8}$$

$$u_i = -\frac{K_{rs_i}}{\mu}K(\nabla p_{s_i} + \rho_{s_i}g) \tag{9}$$

where i represents the number of different phases, s_i represents the saturation or volume fraction of each phase ($s_1 + s_2 = 1$), u_i is the velocity, and K_{rs_i} represents the relative permeabilities. For the wetting phase, the equations used in the Brooks and Corey[47] model are

$$p_c = p_{ec}s_1^{-1/\lambda_p} \tag{10}$$

$$K_{rs_1} = s_1^{3+2/\lambda_p} \tag{11}$$

$$K_{rs_2} = s_2^2(1 - s_1^{1+2/\lambda_p}) \tag{12}$$

where p_c is the capillary pressure and p_{ec} is the entry capillary pressure, which is expressed as $\frac{2\gamma\cos(\theta)}{R_c}$.[48] We have considered θ as a static contact angle. The Whatman grade 4 paper strip used in the present work is superhydrophilic; thus, a value of 0° is considered. A similar value of a superhydrophilic filter paper (0° static contact angle) is also used in the earlier literature.[41,42] The initial value of the volume fraction s_2 is taken as 0.985. To combine the functionality of Darcy's law and phase transport in porous medium interfaces, we used the multiphase flow in porous medium interface. The parameters used to simulate the capillary rise of water in different width paper strips are listed in Table 3.

Table 3. Parameters Used in Simulation for Water

name	value
paper strip width (W_0)	0.005 m, 0.01 m, 0.02 m
paper strip thickness (δ)	0.203 mm
surface tension (γ)	0.072 N/m
pore size distribution index (λ_p)	2
porosity (ϵ)	0.776
permeability (K)	8.67×10^{-12} m^2
density of air (ρ_g)	1 kg/m^3
density of water (ρ)	1000 kg/m^3
viscosity of air	1.76×10^{-5} Pa·s
viscosity of water (μ)	8.9×10^{-4} Pa·s

Analytical Models. Wicking is a spontaneous process where the wetting liquid can flow through any porous medium due to capillary pressure. For predicting the wicking front height, an analytical solution was established, combining the momentum balance equation and Darcy's law, by Masoodi et al.[29] They considered the porous media as a bundle of capillary tubes of the same size and applied the momentum balance method. In momentum balance equations, they considered only the effect of capillary force and viscous resistance. Due to the capillary pressure, the liquid enters the pores, while the viscous force resists the motion. Considering the properties of porous media, the Lucas–Washburn equation is expressed as

$$h = \sqrt{\frac{2Kp_{ec}}{\epsilon\mu}t} \tag{13}$$

where h is the capillary rise height with respect to time t. The Lucas–Washburn (L–W) equation is only valid for a very short period of time because in eq 13, the height is changing linearly with $\sqrt{t}$. The velocity of the liquid in a capillary flow in porous media is decreased with time because of the increasing viscous resistance. Due to this, the flow becomes very slow after a certain time and eventually stops when saturation arises.

https://dx.doi.org/10.1021/acsomega.0c02407
ACS Omega 2020, 5, 22931−22939
RAI Exhibit 2010
Shenzhen Kangvape v. RAI
IPR2024-01406

We have also considered the evaporation model developed by Fries et al.[24] in 2008. Liu et al.[38] also used the same model in the case of a paper matrix. They described the wicking phenomenon in paper by varying the width to measure the capillary rise and weight of the water absorbed. The evaporation rate of the wicking liquid is expressed as

$$m_{ev}^{*} = (1 - \phi) \times p_w \times \frac{0.089 + 0.0782\, V_a}{L_v} \tag{14}$$

where m_{ev}^{*} is the evaporation rate, p_w is the liquid saturated pressure, ϕ is the relative humidity, V_a is the airflow rate, and L_v is the latent heat of vaporization of the liquid. Using eq 14, the total evaporated mass can be calculated at every instant of time, and by subtracting this from the L−W mass, the modified evaporation capillary rise height is obtained as

$$h_{ev} = 2N \cdot e^{-Mt} \int_0^{\sqrt{t}} e^{Mt^2} dt \tag{15}$$

$$M = \frac{2m_{ev}^{*}}{\rho \epsilon \delta} \tag{16}$$

$$N = \sqrt{\frac{\gamma \cos(\theta) K}{\mu \epsilon R_c}} \tag{17}$$

where δ is the thickness of the porous media. We used the Runge−Kutta (RK4) method in MATLAB to solve the differential equation of h_{ev}. The initial value is taken as h_{ev} = 0 when t = 0. Other parameters used in this study are listed in Table 4.

Table 4. Parameters Used in the Evaporation Model for Water

name	value
temperature (T)	26 ± 1 °C
relative humidity (ϕ)	70%
paper strip thickness (δ)	0.203 mm
water saturated pressure (p_w)	4242.85 Pa
airflow rate (V_a)	0
latent heat of vaporization (L_v)	2410 kJ/kg

The general equation of wicking of liquid in a paper strip can be modeled considering the effect of inertial force, capillary force, viscous resistance, and gravitational force.[49] The momentum balance equation considering all of these forces can be written as

$$-\rho \frac{d(h\dot{h})}{dt} = -\frac{2\gamma \cos\theta}{R_c} + \frac{8\,\mu h \dot{h}}{R_c^2} + \rho g h \tag{18}$$

where $\dot{h} = dh/dt$ represents the rate of change of the capillary rise height. Due to the drawbacks of the L−W model here, we further modified the general momentum balance equation considering the effect of gravity in the imbibition phenomenon. We included the gravitational term with the L−W model for describing the capillary rise at a higher time interval.[25−27] At the initial stage, gravity is not a relevant term, but with the rising height, the effect of gravitational force becomes significant. Therefore, we added the gravitational force term to the viscous resistance term and modified the L−W model (the inertial term is neglected for long time analysis). From eq 18, we obtained the modified equation as

$$h\frac{dh}{dt} = \frac{R_c \gamma \cos\theta}{4\mu}\left[1 - \frac{h}{L_{ss}}\right] \tag{19}$$

here, L_{ss} is dependent on gravity. By using the initial condition as h = 0 at t = 0, the solution of eq 19 can be written as

$$h = \frac{p_{ec}}{\rho g}[1 + W(-e^{-\rho^2 g^2 R_c^2 t/8\pi p_{ec} - 1})] \tag{20}$$

where $W(x)$ is the Lambert function. It should be noted that the model including evaporation and gravitational term can be used to predict the initial part of the imbibition (up to few seconds). However, it fails to predict the long duration imbibition process. We have not included this model; rather, we have discussed about the regime-based model in the Results and Discussion section.

AUTHOR INFORMATION

Corresponding Author

Pallab Sinha Mahapatra − *Department of Mechanical Engineering, IIT Madras, Chennai 600036, India;* orcid.org/0000-0002-4073-9980; Phone: +44 2257 4692; Email: pallab@iitm.ac.in

Author

Subhashis Patari − *Department of Mechanical Engineering, IIT Madras, Chennai 600036, India;* orcid.org/0000-0003-2043-5960

Complete contact information is available at: https://pubs.acs.org/10.1021/acsomega.0c02407

Notes

The authors declare no competing financial interest.

ACKNOWLEDGMENTS

S.P. acknowledges the funding received from the Prime Ministers Research Fellowship (PMRF). The authors want to acknowledge the financial support from the Indian Institute of Technology Madras (project number MEE1718695NFSC-PALL and MEE0008846RMFXPALL).

REFERENCES

(1) Woolley, A. T.; Mathies, R. A. Ultra-high-speed DNA fragment separations using microfabricated capillary array electrophoresis chips. *Proc. Natl. Acad. Sci. U.S.A.* **1994**, *91*, 11348−11352.

(2) Barker, S. L.; Tarlov, M. J.; Canavan, H.; Hickman, J. J.; Locascio, L. E. Plastic microfluidic devices modified with polyelectrolyte multilayers. *Anal. Chem.* **2000**, *72*, 4899−4903.

(3) Morrissette, J. M.; Mahapatra, P. S.; Ghosh, A.; Ganguly, R.; Megaridis, C. M. Rapid, self-driven liquid mixing on open-surface microfluidic platforms. *Sci. Rep.* **2017**, *7*, No. 1800.

(4) Martinez, A. W.; Phillips, S. T.; Butte, M. J.; Whitesides, G. M. Patterned paper as a platform for inexpensive, low-volume, portable bioassays. *Angew. Chem., Int. Ed.* **2007**, *46*, 1318−1320.

(5) Nilghaz, A.; Wicaksono, D. H.; Gustiono, D.; Majid, F. A. A.; Supriyanto, E.; Kadir, M. R. A. Flexible microfluidic cloth-based analytical devices using a low-cost wax patterning technique. *Lab Chip* **2012**, *12*, 209−218.

(6) Neethirajan, S.; Kobayashi, I.; Nakajima, M.; Wu, D.; Nandagopal, S.; Lin, F. Microfluidics for food, agriculture and biosystems industries. *Lab Chip* **2011**, *11*, 1574−1586.

(7) Busa, L. S. A.; Mohammadi, S.; Maeki, M.; Ishida, A.; Tani, H.; Tokeshi, M. Advances in microfluidic paper-based analytical devices for food and water analysis. *Micromachines* **2016**, *7*, No. 86.

RAI Exhibit 2010
Shenzhen Kangvape v. RAI
IPR2024-01406

(8) Li, Z.; Rabnawaz, M. Fabrication of Food-Safe Water-Resistant Paper Coatings Using a Melamine Primer and Polysiloxane Outer Layer. *ACS Omega* **2018**, *3*, 11909−11916.
(9) Nguyen, T.-T. T.; Huy, B. T.; Lee, Y.-I. Disposable Colorimetric Paper-Based Probe for the Detection of Amine-Containing Gases in Aquatic Sediments. *ACS Omega* **2019**, *4*, 12665−12670.
(10) Carrell, C.; Kava, A.; Nguyen, M.; Menger, R.; Munshi, Z.; Call, Z.; Nussbaum, M.; Henry, C. Beyond the lateral flow assay: A review of paper-based microfluidics. *Microelectron. Eng.* **2019**, *206*, 45−54.
(11) Hua, M. Z.; Li, S.; Wang, S.; Lu, X. Detecting chemical hazards in foods using microfluidic paper-based analytical devices (μPADs): The real-world application. *Micromachines* **2018**, *9*, No. 32.
(12) Bruzewicz, D. A.; Reches, M.; Whitesides, G. M. Low-cost printing of poly (dimethylsiloxane) barriers to define microchannels in paper. *Anal. Chem.* **2008**, *80*, 3387−3392.
(13) Martinez, A. W.; Phillips, S. T.; Carrilho, E.; Thomas, S. W., III; Sindi, H.; Whitesides, G. M. Simple telemedicine for developing regions: camera phones and paper-based microfluidic devices for real-time, off-site diagnosis. *Anal. Chem.* **2008**, *80*, 3699−3707.
(14) Martinez, A. W.; Phillips, S. T.; Wiley, B. J.; Gupta, M.; Whitesides, G. M. FLASH: a rapid method for prototyping paper-based microfluidic devices. *Lab Chip* **2008**, *8*, 2146−2150.
(15) Cheng, C.-M.; Martinez, A. W.; Gong, J.; Mace, C. R.; Phillips, S. T.; Carrilho, E.; Mirica, K. A.; Whitesides, G. M. Paper-based ELISA. *Angew. Chem., Int. Ed.* **2010**, *49*, 4771−4774.
(16) Sen, U.; Chatterjee, S.; Sinha Mahapatra, P.; Ganguly, R.; Dodge, R.; Yu, L.; Megaridis, C. M. Surface-wettability patterning for distributing high-momentum water jets on porous polymeric substrates. *ACS Appl. Mater. Interfaces* **2018**, *10*, 5038−5049.
(17) Chatterjee, S.; Sinha Mahapatra, P.; Ibrahim, A.; Ganguly, R.; Yu, L.; Dodge, R.; Megaridis, C. M. Precise liquid transport on and through thin porous materials. *Langmuir* **2018**, *34*, 2865−2875.
(18) Cardoso, T. M. G.; Channon, R. B.; Adkins, J. A.; Talhavini, M.; Coltro, W. K.; Henry, C. S. A paper-based colorimetric spot test for the identification of adulterated whiskeys. *Chem. Commun.* **2017**, *53*, 7957−7960.
(19) Shahvar, A.; Saraji, M.; Gordan, H.; Shamsaei, D. Combination of Paper-based thin film microextraction with smartphone-based sensing for sulfite assay in food samples. *Talanta* **2019**, *197*, 578−583.
(20) Puangbanlang, C.; Sirivibulkovit, K.; Nacapricha, D.; Sameenoi, Y. A paper-based device for simultaneous determination of antioxidant activity and total phenolic content in food samples. *Talanta* **2019**, *198*, 542−549.
(21) Darcy, H. *The Public Fountains of the City of Dijon*; Dalmont: Paris, 1856; Vol. *647*.
(22) Washburn, E. W. The dynamics of capillary flow. *Phys. Rev.* **1921**, *17*, No. 273.
(23) Schoelkopf, J.; Gane, P. A.; Ridgway, C. J.; Matthews, G. P. Practical observation of deviation from Lucas-Washburn scaling in porous media. *Colloids Surf., A* **2002**, *206*, 445−454.
(24) Fries, N.; Odic, K.; Conrath, M.; Dreyer, M. The effect of evaporation on the wicking of liquids into a metallic weave. *J. Colloid Interface Sci.* **2008**, *321*, 118−129.
(25) Hamdaoui, M.; Fayala, F.; Nasrallah, S. B. Dynamics of capillary rise in yarns: Influence of fiber and liquid characteristics. *J. Appl. Polym. Sci.* **2007**, *104*, 3050−3056.
(26) Hamdaoui, M.; Nasrallah, S. B. Capillary rise kinetics on woven fabrics-Experimental and theoretical studies. *Indian J. Fibre Text. Res.* **2015**, *40*, 150−156.
(27) Li, K.; Zhang, D.; Bian, H.; Meng, C.; Yang, Y. Criteria for applying the Lucas-Washburn law. *Sci. Rep.* **2015**, *5*, No. 14085.
(28) Chang, S.; Kim, W. Dynamics of water imbibition through paper with swelling. *J. Fluid Mech.* **2020**, *892*, A39.
(29) Masoodi, R.; Pillai, K. M.; Varanasi, P. P. Darcy's law-based models for liquid absorption in polymer wicks. *AIChE J.* **2007**, *53*, 2769−2782.
(30) Rath, D.; Sathishkumar, N.; Toley, B. J. Experimental measurement of parameters governing flow rates and partial saturation in paper-based microfluidic devices. *Langmuir* **2018**, *34*, 8758−8766.
(31) Rayaprolu, A.; Srivastava, S. K.; Anand, K.; Bhati, L.; Asthana, A.; Rao, C. M. Fabrication of cost-effective and efficient paper-based device for viscosity measurement. *Anal. Chim. Acta* **2018**, *1044*, 86−92.
(32) Kar, S.; Das, S. S.; Laha, S.; Chakraborty, S. Microfluidics on Porous Substrates Mediated by Capillarity Driven Transport. *Ind. Eng. Chem. Res.* **2020**, *59*, 3644−3654.
(33) Ravi, S.; Dharmarajan, R.; Moghaddam, S. Measurement of capillary radius and contact angle within porous media. *Langmuir* **2015**, *31*, 12954−12959.
(34) Masoodi, R.; Pillai, K. M.; Varanasi, P. P. In *Role of Hydraulic and Capillary Radii in Improving the Effectiveness of Capillary Model in Wicking*; ASME 2008 Fluids Engineering Division Summer Meeting Collocated with the Heat Transfer, Energy Sustainability, and 3rd Energy Nanotechnology Conferences, 2008; pp 251−259.
(35) Roh, H.-S.; Raspet, R.; Bass, H. E. Parallel capillary-tube-based extension of thermoacoustic theory for random porous media. *J. Acoust. Soc. Am.* **2007**, *121*, 1413−1422.
(36) Zhong, Z. W.; Wang, Z. P.; Huang, G. X. D. Investigation of wax and paper materials for the fabrication of paper-based microfluidic devices. *Microsyst. Technol.* **2012**, *18*, 649−659.
(37) Jafry, A. T.; Lim, H.; Kang, S. I.; Suk, J. W.; Lee, J. A comparative study of paper-based microfluidic devices with respect to channel geometry. *Colloids Surf., A* **2016**, *492*, 190−198.
(38) Liu, Z.; Hu, J.; Zhao, Y.; Qu, Z.; Xu, F. Experimental and numerical studies on liquid wicking into filter papers for paper-based diagnostics. *Appl. Therm. Eng.* **2015**, *88*, 280−287.
(39) Hong, S.; Kim, W. Dynamics of water imbibition through paper channels with wax boundaries. *Microfluid. Nanofluid.* **2015**, *19*, 845−853.
(40) Rasi, M. *Permeability Properties of Paper Materials*; Research Report, Department of Physics, University of Jyväskylä, 2013.
(41) Castro, C. Imbibition in Paper-Based Microfluidic Devices. Ph.D. Thesis, UC Riverside, 2016.
(42) Madhu, N. T.; Resmi, P.; Pradeep, A.; Babu, T. S. Design and simulation of fluid flow in paper based microfluidic platforms. *IOP Conf. Ser.: Mater. Sci. Eng.* **2019**, *577*, No. 012104.
(43) Kumar, A.; Pramanik, S.; Mishra, M. In *COMSOL Multiphysics Modeling in Darcian and Non-Darcian Porous Media*, Proceedings of the 2016 COMSOL Conference; Bangalore, India, 2016; 20−21.
(44) Datta, A. K. Porous media approaches to studying simultaneous heat and mass transfer in food processes. I: Problem formulations. *J. Food Eng.* **2007**, *80*, 80−95.
(45) Halder, A.; Datta, A. K. Surface heat and mass transfer coefficients for multiphase porous media transport models with rapid evaporation. *Food Bioprod. Process.* **2012**, *90*, 475−490.
(46) Chen, Z.; Huan, G.; Ma, Y. *Computational Methods for Multiphase Flows in Porous Media*; SIAM, 2006; Vol. *2*.
(47) Brooks, R. H.; Corey, A. T. Properties of porous media affecting fluid flow. *J. Irrig. Drain. Div.* **1966**, *92*, 61−90.
(48) Masoodi, R.; Pillai, K. A general formula for capillary suction-pressure in porous media. *J. Porous Media* **2012**, *15*, 775−783.
(49) Masoodi, R.; Pillai, K. M. *Wicking in Porous Materials: Traditional and Modern Modeling Approaches*; CRC Press, 2012.

https://dx.doi.org/10.1021/acsomega.0c02407
ACS Omega 2020, 5, 22931−22939

RAI Exhibit 2010
Shenzhen Kangvape v. RAI
IPR2024-01406